Lasers in Medical Science
https://doi.org/10.1007/s10103-021-03383-1

ORIGINAL ARTICLE

Monte Carlo simulations of photodynamic therapy in human blood model

R. S. Alanazi[1,2] · A. Laref[1]

Received: 18 May 2020 / Accepted: 19 July 2021

Abstract

This study aims to simulate a therapeutic plan for a normal human blood model under various patho-physiological conditions, such as the development of leukemia/blood diseases, by means of Monte Carlo multilayered simulation. The photosensitizing compound selectively accumulates in the target cells. A superficial treatment of a blood sample was performed at different ratios of oxygen saturation ($f_{oxy} = 50\%, 53\%, 55\%, 60\%, 65\%, and 70\%$) under the concentration ($C_{MC540} = 30$ μM) effect of merocyanine 540 (MC540) in the blood irradiation. This was done under the application of visible light of wavelength ~ 580nm at an exposure time ~ 60 s. The dose of photodynamic therapy (PDT) was evaluated for the biological damage, leading to necrosis and blood damage during the treatment. In addition, the effect of PDT treatment response in the blood is related to hemoglobin oxygen saturation, resulting in an excellent relationship between the changes caused by the treatment in the blood at a peculiar oxygen saturation rate (for the highest response: $f_{oxy} = 50\%$) and a light dose (LD) of 3.83 Jcm^{-2} above the minimal toxicity of normal tissues. The photodynamic dose is related to the depth of necrosis and the time of treatment for the achievement of the LD delivery at the PDT of blood.

Keywords Photodynamic therapy · Blood irradiation · Light dose · Blood necrosis · Photodynamic dosimetry · Oxygen saturation · Leukemia disease

Introduction

Cancer persists as a global health issue, which represents the predominantly influencing disease on the universal health and elevated mortality rate. This is mainly due to the malignancy, which remains the leading cause of death [1–18]. For this main reason, an alternative therapy is useful to fight malignant diseases, which is less harmful when compared with chemotherapy or radiotherapy. In this regard, photodynamic therapy (PDT) is a convenient tool that involves the use of a photosensitizer. This has the ability to be localized in the region of tumors or lesions in the tissue. Therefore, the various malignant and non-malignant diseases can be treated [3–25]. The light source type is often chosen based on the depth of the lesion or tumor with the requirement of the light dose (LD) and the photosensitizer [26]. The illumination must be enough for the treatment of the selected area, while the irradiance must be sufficiently high to offer a better treatment response. Most importantly, the wavelengths should match the absorption bands of the photosensitizer [27]. Hence, the activation of the photosensitizer can be achieved through the exposure to the light at a special wavelength, while the energy is transferred through the excited sensitizer into a molecular oxygen. This is conducive for the generation of toxic oxygen, which is recognized as the oxidized root species [4]. Thus, the singlet oxygen represents the essential vehicle of the therapy impact of PDT to cure the local damage. The apoptosis/necrosis forms of tumor cells and immunogenic cell death ultimately lead to the remission of tumor [5].

Photodynamic reactions represent a multistage process, which involve a triple-element photochemical interaction with light, photosensitizer, and oxygen [20, 21]. This can lead to the tissue damage in two types of interaction. In the first type of reaction, the excited state of the photosensitizer reacts simply with a number of organic substrates or the

✉ A. Laref
la_amel@hotmail.com

[1] Department of Physics and Astronomy, College of Science, King Saud University, Riyadh 11451, Saudi Arabia

[2] Department of Biomedical Technology, College of Applied Medical Sciences, King Saud University, P.O. Box 10219, Riyadh, Saudi Arabia

Published online: 28 August 2021

presence of the solvents in the tissue. This can conduct to the produced cytotoxic of free radicals through an electron or a proton transfer in order to generate radical species [22]. The second one involves another interaction that is more common for the photodynamic effect and is produced via the singlet oxygen. The physical processes involve singlet oxygen ($^1O2$) generation reactions, which are described in the previous reports [21–25]. Most oxygen reactions have harmful effects on the cells and surrounding cell structures, which can undergo an irrevocable reaction. The reaction of singlet oxygen with blood indicates the chief cause of cellular damage through a photodynamic effect, and the damage would have the form of blood necrosis, which conducts to its death [22]. The application of PDT in blood is feasible, such as in leukemic and acute promyelocytic leukemia (HL-60), as well as normal bone marrow cells. Also, the treatment of acute lymphoblastic leukemia continues to evolve into a mature clinical treatment modality. It is then considered as a promising approach for eradicating blood diseases [6, 7]. For this purpose, in the present work, an extensive update on the use of PDT in cancer research and treatment is initiated, and the application of this approach is discussed to support leukemia therapy.

Optical property measurement can be performed in human blood via the visible light when the photosensitizer is stimulated. The accumulation of the photosensitizer matter of merocyanine 540 (MC540) can absorb in visible light of $\lambda = 580nm$, while the penetration depth of the light significantly relies on the scattering and absorption features of the blood. Hence, the fraction volume of blood with oxygen saturation [8] has higher optical penetration depths ($\delta = 0.01192\ cm$ at $f_{oxy} = 50\%$) to increase the treatment depth in blood [5]. The plan of the treatment requires the measured optical properties in a human blood sample as part of a PDT simulation. The deeper blood penetration of visible light of $\lambda = 580nm$ is compared to shorter wavelengths of light. This can render the visible light dose more suitable for the PDT treatment, involving profound targets and thick lesions [9]. The PDT was simulated at a visible light of $\lambda = 580nm$ using fluence rates of $12.7, 25.47, 38.21, 50.95, 63.69, 76.43, and 89.17 mWcm^{-2}$ at seven LDs of 0.76, 1.52, 2.29, 3.05, 3.83, 4.58, and 5.35 Jcm^{-2}, respectively. The seven LDs are compared in terms of local damage (irreversible damage), which is indicated by the smallest of the seven local damages acquired at the profound zone of the blood sample dimensions [μm]. Therefore, it is possible to estimate the treatment times ($t_n = 5.65, 2.83, 1.89, 1.42, 1.15, 0.95, and 0.85s$) that are required for the fluence rates of the seven prior LDs to establish the reference damage. This was certainly effective for surface treatment, which is very safe for many blood diseases with response rates at a LD = 3.83 Jcm^{-2}. A photodynamic dose is indicted by the total cumulative of singlet oxygen created along the treatment, which is incorporated at $= 9 \times 10^{17}\ photon/g > D_{th} = 8.6 \times 10^{17} photon/g$. This photodynamic dose relies on the total rate of local fluence, which is determined through the summation of the local diffusing fluence rate and the local incident fluence rate. Also, the absorption coefficient is used for the MC540 to estimate the local damage caused by PDT.

In this work, a model is proposed for the PDT process to treat the blood sample. The Monte Carlo (MC) technique is used to investigate the light penetration depth and fluence rate at various values of diminished scattering (μ_s) and absorption (μ_a) coefficients by using a source emission of point light from the spherical diffuser at a wavelength of $\lambda = 580nm$. This corresponds mainly to the MC540 for the light-sensitive material. Also, the impact of variability of optical, geometric, and diffuser-relying parameters on the delivering of dose into the target volume is established [10]. The simulated results make it possible to establish a model, conducting to the diagnosis of blood diseases possible at the surface irradiation. The photodynamic threshold of normal blood is calculated at different concentrations of oxygen saturation with MC540 to estimate the PDT-induced blood necrosis (z_n). The light fluence distribution during the PDT and photosensitizer uptakes in the visible light. The simulated results of a blood sample show that a laser of wavelength of $\lambda = 580nm$ and the dose $D = 9 \times 10^{17}$ photon/g are very high to achieve blood necrosis at $Z_n = 63\mu m$. Higher light fluence rates enabled a shorter $t_n = 1.15$ s to be achieved for intraoperative irradiation times with no loss of efficiency.

Materials and methods

Blood optical properties

The current study includes a blood sample (comprising both oxy-hemoglobin and deoxy-hemoglobin) with a volume fraction of blood (B) possessing a total oxygen saturation (f_{oxy}), as indicated by the summation of the individual absorption coefficients of the components. All related parameters are

Table 1 Optical properties of normal human blood model [13]

Wavelength λ [nm]	Oxygenated ($H = 0.45\%$)		Deoxygenated ($H = 0.45\%$)		g	n	$\rho[\frac{g}{cm^3}]$
	$\mu_{oxy}a(\lambda)[\mathbf{cm}^{-1}]$	$\mu_{dxy}a(\lambda)[\mathbf{cm}^{-1}]$	$\mu_{oxy}a(\lambda)[\mathbf{cm}^{-1}]$	$\mu_{dxy}a(\lambda)[\mathbf{cm}^{-1}]$			
580 nm	224.8	176.9	3291.1	3126.7	0.988	1.33	1.060

listed in Table 1, with the optical coefficients, fluence rate build up at anisotropy ($g = 0.988$), and refractive indices of the blood ($n = 1.33$) [11].

$$\mu_a(\lambda) = f_{oxy}\mu_{oxy}(\lambda) + (1 - f_{dxy})\mu_{dxy}(\lambda) \tag{1}$$

where $\mu_{oxy}(\lambda)$ and $\mu_{dxy}(\lambda)$ are indicated by the absorption coefficients of deoxygenated (oxygen saturation = 0%) and oxygenated (oxygen saturation = 100%) blood, respectively, and W_{HRB} [g/L] represents the concentration of total hemoglobin, as defined by Eqs. (2) and (3). In addition, the total oxygen saturation O_2 is defined by Eq. (4) [12].

$$\mu_{oxy}(\lambda) = \frac{2.303 * e_{oxy}(\lambda) * C_{hem}}{W_{HRB}} \tag{2}$$

$$\mu_{dxy}(\lambda) = \frac{2.303 * e_{dxy}(\lambda) * C_{hem}}{W_{HRB}} \tag{3}$$

$$O2 = \frac{[HbO2]}{[HbO2] + [HO2]} \tag{4}$$

where $[HbO2]$ and $[Hb]$ are described by the concentrations of oxy-hemoglobin and deoxy-hemoglobin, respectively, in the total blood volume, i.e., all blood located in the capillary, arterial, and venous compartments. The scattering coefficients of deoxygenated (μ_{dxys}) and oxygenated (μ_{oxs}) total blood were calculated by means of Mie theory. It was assumed that the independent scattering of particles occurs in the whole blood. The obtained results exhibited an analogous spectral shape compared to the previous reports with noticeably bigger values. The main reason relates to the densely packed erythrocytes in the whole blood, whereas the optical scattering is no longer independent of the blood cells. Finally, the normal physiological value $H = 0.45$ and the packing factor $W = 0.3$ are undertaken [13]. The total reduced scattering coefficient (μ_s) for blood is expressed by Eq. (5) [13].

$$\mu_s = W(f_{oxy} * \mu_{oxs} + (1 - f_{oxy}) * \mu_{dxys}) \tag{5}$$

where μ_{oxs} and μ_{dxys} are the decreased scattering coefficients of oxygenated and deoxygenated blood, respectively.

Figure 1 clearly shows that the peak in the hemoglobin (Hb and $Hb0_2$) absorption is located at ~ 580 nm, which is used in the treatment. The scattering ($\mu_s = 986.8\ cm^{-1}$) and absorption ($\mu_a = 224.32 cm^{-1}$) coefficient values are extracted at 580 nm.

Photosensitizers

The photosensitizers work as exogenous fluorophores, which induce the fluorescence in the target tissues indirectly when the intrinsic fluorophores are not adequate for the desired application. The design is based on having a big singlet oxygen quantum yield to achieve phototoxicity in PDT. The selection of an appropriate photosensitizer is based on increasing the depth of the excitation light penetration at high absorption light transformers with longer wavelengths to reach the appropriate processing depth [14]. The photosensitizer MC540 used in this study is based on the optimal uptake by the target leukemic cells, some categories of immature blood cells, and photophysical properties [15, 16]. MC540 is a cheap and readily accessible anionic cyanine dye in which the absorption of light is located in the visible span [17]. The absorption and fluorescence properties of MC540 can be dissolved in ethanol. For MC540, the longest wavelength absorption band is approximately 560 nm, and the excitation wavelength is

Table 2 Main fluorophores contributing in MC540 for PDT [19]

Fluorophore	Max excitation $\lambda[nm]$	Max emission $\lambda[nm]$	Application
Merocyanine 540	560	580	Leukemia, lymphoma

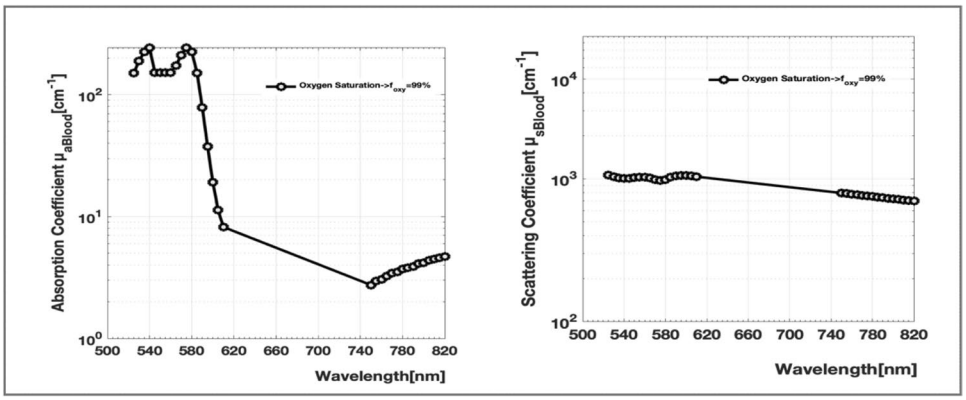

Fig. 1 Absorption coefficient and scatter coefficient spectra for blood at $f_{oxy} = 99\%$

530 nm. The quantum yield of this molecule is 0.39 [18]. All main parameters for MC 540 that are useful in PDT are summarized in Table 2.

Light sources

For the production of an adequate amount of singlet oxygen and for the prediction of the necrotic zones in PDT, MC simulation provides practical techniques for the computation of light distributions in biological tissues. This can rely on simple expressions of spherical, cylindrical, and planar geometries from the point sources [28]. The light sources and the blood sample were characterized by a homogeneous model (with a diameter of 120 µm and thickness $Z = 400$ µm blood vessel compressing either blood at 45% hct [29, 30]) and were initially used to acquire the distribution of scattering/absorption events within a normal blood sample and the photosensitizer MC540. The calculations were carried out by employing MC multilayered (MCML) code [31, 32]. In the simulation, total photon packets of ~10^4*photons* were set at the visible-light laser with a wavelength $\lambda = 580nm$ that is used in PDT. This is mainly produced from a point source of the unit at a maximum power $P = 50mW$ and a spot of radius $r = 5mm$. In this case, the blood was irradiated at a surface energy of $4Jcm^{-2}$, and the fluence rate did not exceed $F = 100mWcm^{-2}$. Here, the photons were distributed in a spherical shape along the z-axis pointed into the sample. The simplified blood sample model consists of data taken from previous work [13]. A section with a thickness of 400 µm includes a designed model of the blood sample, as displayed in Fig. 2. The important parameters used in this study regarding the LD and photosensitizers (MC450) are presented in Table 3.

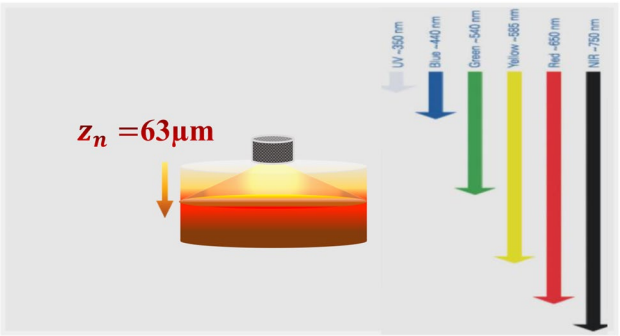

Fig. 2 Geometrical structure of the laser source as a point with a 5-mm-diameter laser beam ($\lambda = 580$ nm) and radiant exposure $E = 64$ mWcm^{-2} at the center, which is illuminated on the top, and the photons propagating down in a spherical diffusion on sample blood with the MC540 are accumulated and assumed to be of uniform density

Diffusion model of the fluence rate distribution

To describe the absorption and scattering characteristics of the medium, the most regularly extracted optical interaction coefficients are indicated by the effective attenuation coefficient, $\mu_{eff}(cm^{-1})$, and its corresponding inverse, which represents the penetration depth and is denoted by $\delta = 1/\mu_{eff}$ [33]. It is described by the incremental depth in the tissue where the fluence rate collapses into 1/e of its preceding value. Once the effective attenuation coefficient is revealed, then the relative distribution of energy fluence is predictable in such a medium. The effective attenuation coefficient is itself related to the absorption and diminished dispersion factors. This relation is illustrated in Eq. (6) [34].

$$\mu_{eff}^2 = 3\mu_a(\mu_a + \mu_s') \tag{6}$$

Although μ_{eff} is the most simply established from the optical interaction coefficients, its determination does not make the absolute distribution of the energy fluence rate in tissue predictable [35]. According to the principle of the diffusion of light in tissue, many different "geometries" are possible for the light irradiation in PDT, as portrayed in Fig. 3. Surface radiation that involves a superficial treatment of the light source is exterior to the body, or it can illuminate the interior surface of a body cavity [36], as expressed by Eq. (2).

$$\phi = \phi_0 k e^{(-\mu_{eff} z)} \tag{7}$$

Table 3 Light dose (LD) and photosensitizers examined for MC450

	Definition	Parameter
Photons	Wavelength	$\lambda = 580nm$
	Irradiance	$E = 64mWcm^{-2}$
	Exposure time	$T = 60$ s
	Optical penetration depth	$\delta = 0.01192$ cm
	Optical backscatter factor	$k = 4.4$
Photosensitive drug	Extinction coefficient of drug	$\varepsilon = 32783cm^{-1}(mg/ml)$
	Quantum efficiency	$\phi = 0.39$
	MC540 concentration of drug	$C_{MC540} = 30\mu M$
Blood	Blood density	$1.016g/cm^3$

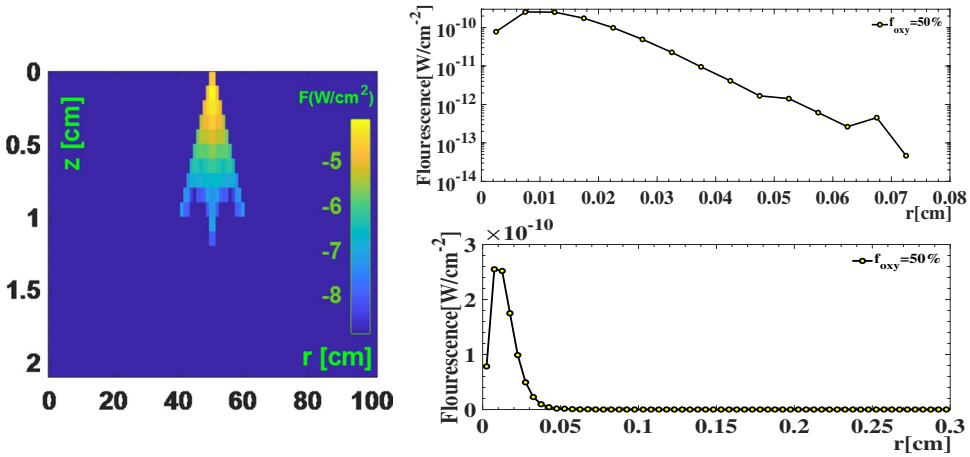

Fig. 3 Typical fluence rate F Wcm^{-2} distributions during PDT calculated using MC simulations by assuming $\mu_a = 200.85\ cm^{-1}$ and $\mu_s = 962.6\ cm^{-1}$

where $\phi[(Wcm^{-2})]$ represents the energy fluence rate for a surface irradiance of $\phi_0([Wcm^{-2}])$ that can penetrate at a specific depth z[cm]. Here, k [no unit] is a factor that relies on the tissue absorption and scattering coefficients by applying a treatment wavelength to the tissue surface, which can result from the effect of the backscattered light near the tissues [33].

Equation (8) indicates the emission from a point source by providing a radiant power P ($[mW]$). This can be expressed according to the diffusion theory, which is described via the relation between the energy fluence rate, $\phi([Wcm^{-2}])$ at a distance r [cm], the diminished scattering coefficient $\mu_s^{'}(cm^{-1})$, and the absorption coefficient within an infinite turbid medium $\mu_a(cm^{-1})$[35].

$$\phi = \left(\frac{P3(\mu_s^{'} + \mu_a)}{4\pi r}\right)e^{(-r/\delta)} \tag{8}$$

Equations (7) and (8) represent the complete representation of the light distribution viable under the two special source geometries, as mentioned earlier, while the values of $\mu_a(cm^{-1})$ and k [no unit] are needed for $\mu_{eff}(cm^{-1})$.

PDT dosimetry

The LD that produces the photodynamic behavior is represented by H [J cm^{-2}], as written by Eq. (9). It indicates fluence rate ϕ[W cm^{-2}] times the exposure time t [s].

$$H = \phi t \tag{9}$$

The PDT treatment can be achieved through a stochastic event, which is governed by the fluence, as given by Eq. (9). This mainly results in the damage caused by the oxidation in the form of "necrosis or apoptosis" when the threshold fluence (H_{th}) value exceeds H [J cm^{-2}], as defined by Eq. (10):

$$H_{th} = Eke^{-Z_{necrosis}/\delta}t \tag{10}$$

The fluence rate H [J cm^{-2}] can reach $H_{th}[(Jcm^{-2})]$ at a depth $Z_{necrosis}[(cm)]$ that corresponds to its effective treatment. The form can be obtained according to Eq. (11).

$$Z_{necrosis} = \delta ln\left(\frac{Etk}{H_{th}}\right) \tag{11}$$

There is a proportionality between $Z_{necrosis}[(cm)]$ and the optical penetration depth (δ) that is linked to a factor via the logarithm function. Therefore, their effect on $Z_{necrosis}$ is reduced by using the variable constants, such as t, E, and k, but the time varies, as provided by Eq. (11) [37].

The expression for the optical penetration depth $\delta[(cm)]$ is expressed in terms of Eq. (12), showing that $\delta[(cm)]$ to be proportional to the geometric mean of μ_a and $\mu_s^{'}$. For $\mu_s^{'} \gg \mu a$, it is usually described for the red to near-infrared light.

$$\delta = \frac{1}{\sqrt{3\mu a \mu s'}} \tag{12}$$

A crucial biological component for obtaining μa is indicated by the blood perfusion. It can readily vary by a factor of 2–4. Thus, the $Z_{necrosis}$ is significantly affected by the inflammation degree in a target tissue. The augmentation of fourfold in blood perfusion would provoke a fourfold augmentation in μa, yielding more than a twofold reduction in δ as well as at least a halving for the treatment depth [38].

The photodynamic dose indicates the absorption of photons number by the photosensitizer, per gram of tissue [photon/J], as written in Eq. (13) [39]. Note that ρ represents the tissue density $[(gcm^{-3})]$, ϕ describes the light fluence rate $[(mWcm^{-2})]$, $h\nu$ denotes the energy of a photon [photon/J], C defines the drug concentration in the tissue [μM], ε indicates the extinction coefficient of the

photosensitizer drug [1/cm/M], and t represents the exposure time. These parameters are selected to influence the dose estimation [40].

$$D = \int_0^t \varepsilon C \frac{\phi(t')}{h\nu} . \frac{1}{\rho} dt' \tag{13}$$

$$D = \varepsilon C T \frac{\phi}{h\nu} . \frac{1}{\rho} \tag{14}$$

Here, a toxic threshold, representing the maximum number of photons that must be absorbed until the occurrence of necrosis, is adopted. The value of *thresholddose* $D_{th} \sim 8.6 \times 10^{17} (photon/g)$ was determined from photon measurements in liver tissue and was selected here for comparison with the previously published models [41].

PDT damage

Tissue responses to the effectiveness of PDT doses are assessed based on the threshold dose [D_{th}], where they indicate survival doses lower than $D_{th}[(\frac{photon}{g})]$. However, the doses above D_{th} necrosis lead to the defectiveness of the treatments [42]. They evaluate the threshold dose that is associated with the penetration of the amount of light in the tissue and its depth. The effects on intact and necrotic tissues rely on the local light fluence and photosensitizer concentration, as well as the local availability of oxygen [43].

To determine the threshold dosimetry of PDT, it is necessary to describe the threshold concentration of oxidizing species created by PDT that elicits the treatment, while $P_{th}[(M]$ is indicated by Eq. (15).

$$P_{th} = H_{th} \varepsilon C \eta f_{kill} \frac{1}{h\nu} T \tag{15}$$

$$P_{th} = D.\eta.f_{kill} \tag{16}$$

The inclusion of the extinction coefficient $\varepsilon[(cm^{-1}M^{-1})]$ for the photosensitizer concentration C [M] is related to the quantum efficiency that converts the excited state of the photosensitizer to the oxidized species $\eta[(nounit)]$. It depends on the availability of oxygen, and the oxidizing species fraction that invade the sites participating to lethality f_{kill} and $h\nu$ is the energy of a photon (photon/J) participating in yielding units of moles per liter [M] for P_{th}.

The rearrangement of Eq. (17) is needed for the resolution of $Z_{necrosis}([cm])$ and the substitution of the depth of optical penetration $\delta([cm])$ for 1/μ yields

$$Z_{necrosis} = \delta ln(\frac{\lambda(1000) Etk\varepsilon C\phi f_{kill}}{N_a h c_0}) \tag{17}$$

The key points from Eqs. (15) and (16) require that the optical properties have a prevailing impact on the region of PDT treatment. Equation (17) indicates that the variations in the blood perfusion can significantly restrict the regional treatment [37, 38].

Results

Measured fluence rates in the blood

To simulate the fluence rate of light, the blood was used as a medium for therapeutic dose accumulation with the addition of different concentrations of oxygen in the blood and the concentration of MC540 was set to C_{MC540}= 30 μM. Its visual properties are collected in Tables 1 and 3 (as taken from a previous report [13]) by positioning the laser (λ = 580 nm), and the surface was located at $Z = 0cm$.

A map of light distributions predicted by diffusion theory simulation for a normal blood sample with MC540 photosensitizer clearly shows that the fluence rate increases at the higher concentration of the ratio of oxygen saturation as a function of the penetration of light. Thus, the depth of penetration increases and indicates a propagation model, as displayed in Fig. 4.

Figure 5 shows the fluorescence of blood at different ratios of oxygen saturation $f_{oxy} = 50\%, 53\%, 55\%, 57\%, 60\%, 65\%, and 70\%$, respectively, at a concentration of the material MC540 of C_{MC540}= 30 μM, and the positioned radiant source is set at $Z = 0cm$ for a laser light of $\lambda = 580nm$. The simulated series were recorded along the tracks positioned at photons of source of $N = 10^4$ photons taken inside the blood. The higher oxygen saturation in the blood led to a decrease in the fluence rate of $F_{max} = 2.6 \times 10^{-10} W/cm^2$ at $f_{oxy} = 50\%$ during the irradiation time $t \sim 60$ s. Two different regions were observed by using MC simulation. The first one, located at range $r = (0 - 0.015)cm$, near the blood surface is known as the accumulation zone (the build-up region). The fluence rate is high up to the maximum values because of the blood absorption properties ($F_{max} = 2.6 \times 10^{-10} W/cm^2$). Therefore, in the second region, the fluence exhibits an exponential decrease as a function of the depth with a diameter maximum of $0.5cm$ at $F_{min} < 2{\times}10^{-10} W/cm^2$, as shown in Fig. 2b.

The effects of different MC540 concentrations were investigated during the phototherapy and the blood damage versus the change of the concentration C_{MC540}. By employing an MC model, the homogeneous distribution of MC540 was observed, and the fluence rate distribution was decomposed with blood depth. Photobleaching altered the spatial distribution of MC540 in the blood. The upper layer (surface

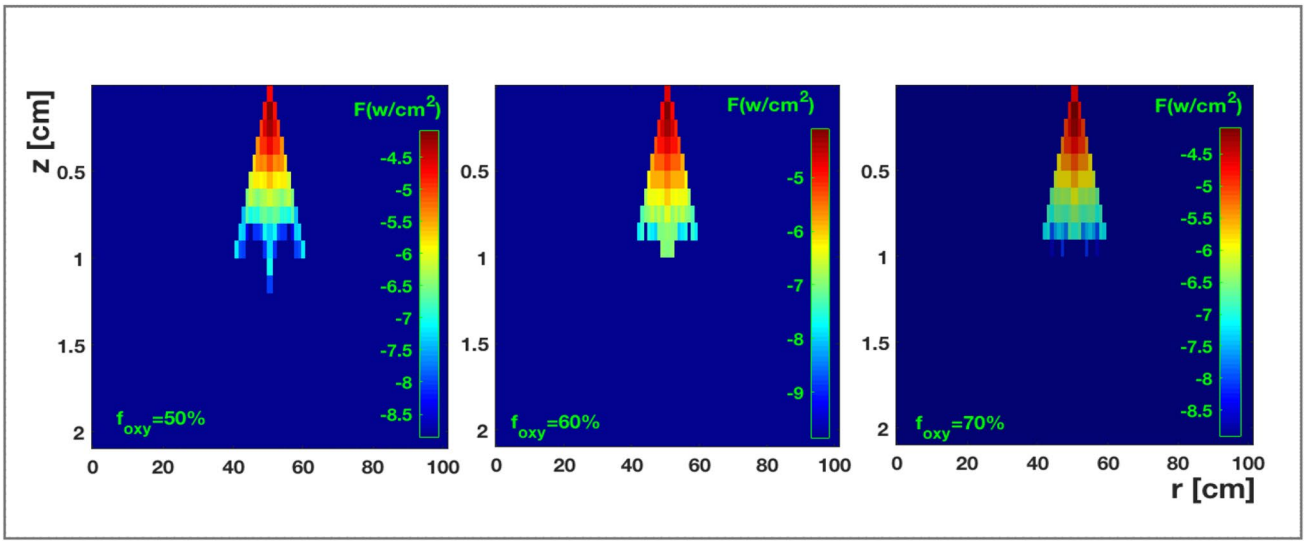

Fig. 4 MC profiles of fluence rate F [(Wcm^{-2}] within a simulated thickness $z=400$ μm for blood vessel filled with blood containing $H=45\%$ hematocrit and relative fractions of blood $B=2\%$: the added MC540 with different oxygen saturation concentrations at values (**a**) $f_{oxy}=50\%$, (**b**) $f_{oxy}=60\%$, and (**c**) $f_{oxy}=70\%$ is plotted as a function of vertical distance z [(cm]) and the lateral distance r ([cm)] from the source

region) experienced the biggest fluence rate. Hence, this will experience the photobleaching promptly. It was suggested that the MC540 concentration of ~ 30 μM has a negligible influence on the absorption coefficient of the blood. Thus, it can result in a time-independent fluence-rate distribution. MC540 photobleaching was assumed to follow a tendency of first-order exponential decay. Its concentration, C_{MC540}, decreased at a rate proportional to the local fluence rate $F[(W/cm^2]$, as shown in Fig. 6. It is possible to record a wide variation in the MC540 fluorescence rate at different oxygen concentrations of f_{oxy}. However, the best concentration of treatment is considered to be within the range of approximately 10–30 μM, as shown in Fig. 6.

PDT is restricted to more-superficial regions because of the limited depth of light penetration. For a monochrome beam of $\lambda = 580$ nm, the absorption spectrum for MC540 has a large activation peak, resulting in a greater absorption and penetration at the surface dose along with treatment depth, as shown in Fig. 7. The PDD is directly related to the photosensitizer concentration and the fluence rate of light as well as oxygen saturation (f_{oxy}) in the blood. The resulting regions with lower power render the treatment ineffective at $LD < 3.83$ J cm^{-2} when the power is less than 50 mW. This can be explained to the fewer absorption events possible to reach the estimated threshold $D_{th} 8.60 \times 10^{17} photon/$ g. However, the absorption is significant in the regions at higher power. The PDD is higher at $LD > 3.83$ J cm^{-2} when the power is greater than 50 mW. This explains the larger spread in PDD in the areas above the threshold. The reported data demonstrated the processing protocol performed at $LD = 3.83$ J cm^{-2} and a power of 50 mW at a concentration $C_{MC540}= 30$ μM for MC540. This finding is expected to kill a large number of direct cells at $PDT = 8.79\times10^{17}$ photon/g with a focused oxygen saturation of $f_{oxy}= 50\%$.

Concentration hemoglobin oxygen saturation

The simulated absorbance of blood is given for a thickness of $Z=400$ μm (taken from previous reports [29, 30]) at a wavelength of visible light of $\lambda = 580$ nm obtained at various oxygen saturations from 50 to 70% for a blood volume fraction of $B=0.002$. As expected, the absorbance changes are the most prominent in the wavelength range varying from 500 to 600 nm. Different ratios of oxygen saturation in the blood are obtained with the blood absorption coefficient, showing a continuously increasing relationship, as depicted in Fig. 8. The light fluence distribution obtained at different blood oxygen saturations (f_{oxy}) resulted in the difference between the absorption coefficients at 580 nm, as summarized in Table 4.

Figure 9 demonstrates the monitoring of typical time behavior for the blood oxygen saturation with the relative hemoglobin concentration ($B=2\%$) by including MC540, which was calculated from the MCML model during PDT. The treatment was started at $t=0$ s and released at $t=60$ s. Under normal conditions, the regular increase in f_{oxy} occurs in the range of 10–90% and at the time up to $t=60$ s, which continues to increase by showing $\mu_a < 200.85 cm^{-1}$ at $f_{oxy}= 50\%$. It is clearly seen that the photons have a longer

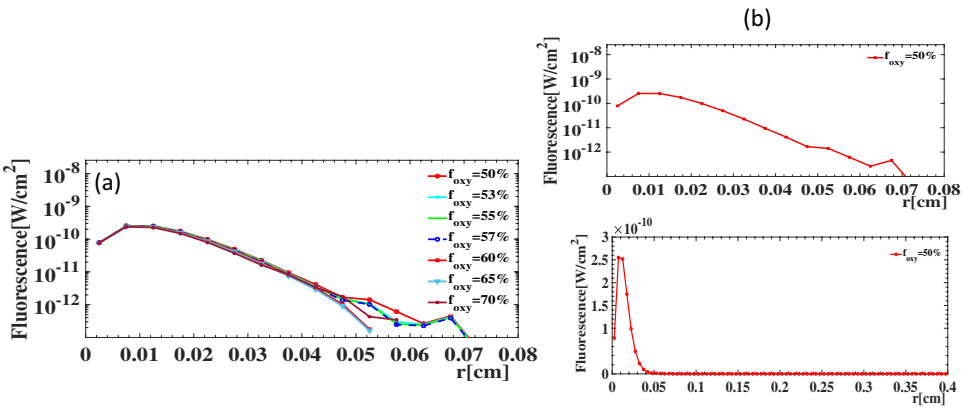

Fig. 5 **a** Fluence rate F [(W/cm^2] as a function of depth r ([cm)] simulated in the blood with photosensitizer MC540 at different oxygen saturation ratios (f_{oxy} = 50%, 53%, 55%, 57%, 60%, 65%, and 70%) and **b** f_{oxy} = 50%

absorption in the visible wavelength = 580 nm for all cases, tending to increase with f_{oxy} in the range of (0 − 100%) through ~ 60 s. However, for a very high absorption of blood at f_{oxy} (50% − 100%)%, the differences in the visible optical path of laser light increase with increasing f_{oxy}. The differences in the optical path of $\lambda = 580nm$ continue to increase with blood oxygen saturation.

The effects of fluence rate on different concentrations of oxygen in the blood with the concentration MC540 are analyzed. For each constriction, the MC540 fluorescence intensity values are recorded at $\lambda = 580$ nm. Figure 10 shows the fluence rate as a function of the depth at different concentrations of oxygen. The fluence rate is defined as the amount of fluence divided by the incident irradiance. This figure exhibits the fluence rate for a certain concentration of oxygen ratio (f_{oxy} = 50%, 53%, 55%, 57%, 60%, 65%, and 70%) at a visible light wavelength of $\lambda = 580nm$, as shown in Fig. 4. The MC540 fluorescence intensity clearly varies at different concentrations of oxygen during the time treatment. As expected, from the outset to the end of treatment, the

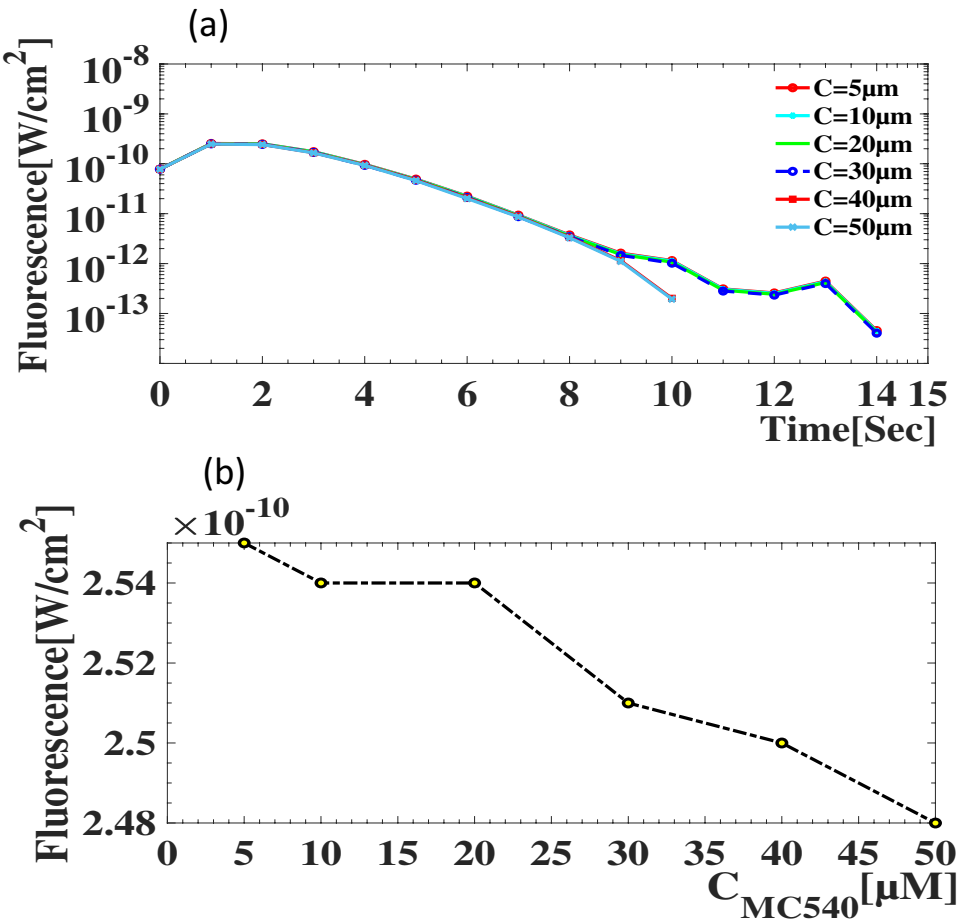

Fig. 6 **a** and **b** The fluence rate in the blood through the period irradiation time t = 60 s at different concentrations of MC540 = 5, 10, 20, 30, 40, and 50 μM as a function of time during the treatment

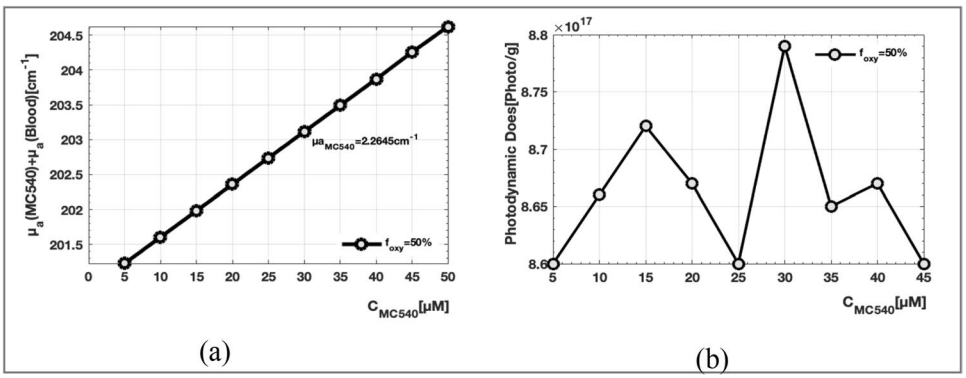

Fig. 7 **a** The relationship of the absorption coefficient MC540 [μa_{MC540}] to C_{MC540} and **b** the photodynamic dose (PDD) that compares the different concentrations of MC540

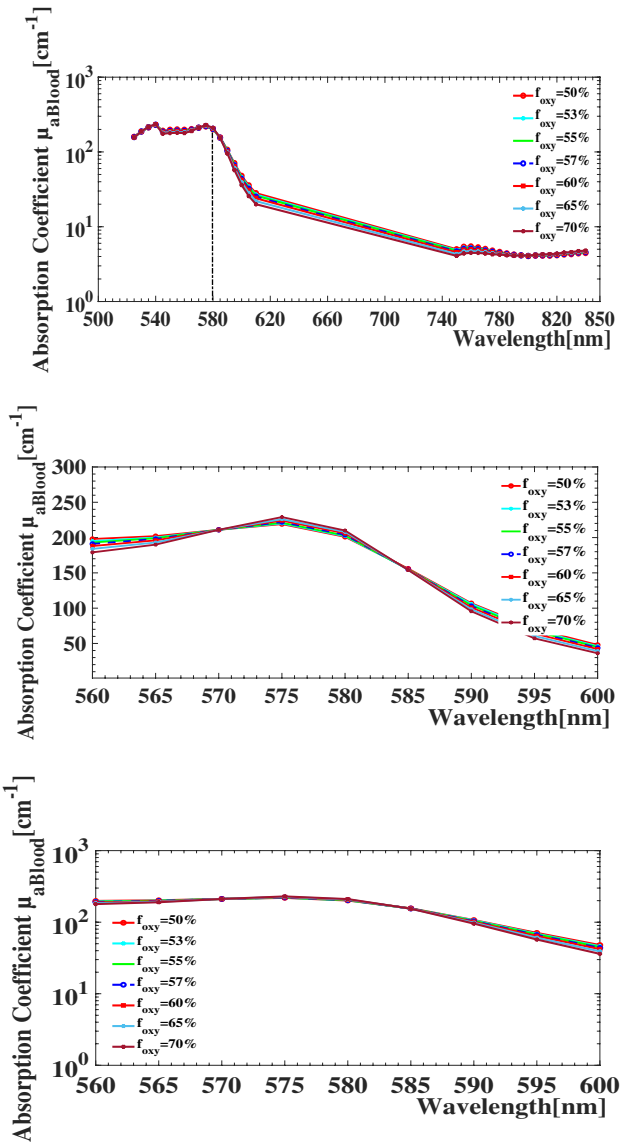

Fig. 8 Attenuation spectra of the blood having MC540 at different oxygen saturations f_{oxy} = 50%, 53%, 55%, 57%, 60%, 65%, and 70%, with a wavelength of λ = 580 nm showing the in vivo distribution of absorption coefficients in normal human blood during the irradiation time $t \sim 60$ s (data taken from previous work [13])

reduction of the fluorescence peak of MC540 is clear until the treatment progresses to the maximum value at approximately $1.41 \times 10^{-10} W/cm^2$ for $f_{oxy} = 50\%$.

Photodynamic therapy

The photodynamic doses versus the exposure time computed at various concentrations of oxygen are plotted in Fig. 11. The PDD increases with the increase of time, and the transmission of light into the blood increases as well. Therefore, the PDT treatment in the blood depends strongly on the concentration of oxygen. Few changes were observed in the spectral shape of the photodynamic dose of blood by changing the concentration of oxygen at $f_{oxy} = 50\%$, especially in the region between $f_{oxy} = 50\%$ and $f_{oxy} = 60\%$. A significant variation in the photodynamic doses of the blood occurs with the increase in the concentration of oxygen along the absorption C_{MC540} at 30 μM, especially at the visible laser ($\lambda = 580nm$). In addition, the maximum value of the therapeutic dose versus the exposure time increases weakly between $f_{oxy} = 60$ and 70% and continues to increase to the maximum value at $f_{oxy} = 50\%$. The absorption coefficient of the substance is fixed to μa_{MC540} during the irradiation period at a wavelength of $\lambda = 580nm$. The concentration of oxygen affected the treatment, which could also explain why the recorded amount of the dose is lower at the concentration $f_{oxy} = 70\%$. This could effectively reduce the amount of the maximum dose that reached the target. In addition, it provided a good opportunity to determine the optimal oxygen concentration in the PDT ($f_{oxy} = 50\%$).

Table 4 Typical optical properties of blood at different f_{oxy} with $C_{MC540} = 30\mu M$ taken at $\lambda = 580nm$.

f_{oxy}	$\mu_a[cm^{-1}]$	$\mu_s[cm^{-1}]$	δ[cm]
50%	203.11	962	0.01192
55%	205.50	965	0.01183
60%	207.90	967.6	0.01175
70%	212.69	972.5	0.01159

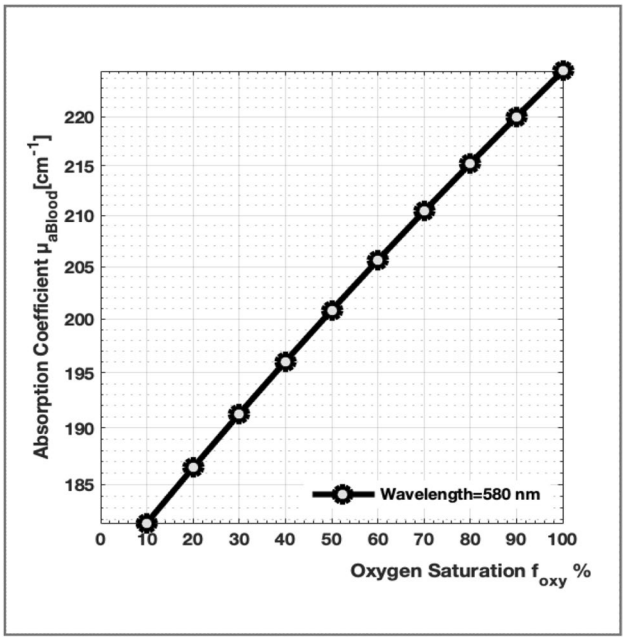

Fig. 9 In vivo, the blood absorption of blood volume ($B = 0.002$) is observed with the distribution of oxygen saturation at different concentrations f_{oxy} $\{0 - > 100\}\%$ using a wavelength of $\lambda = 580$ nm. During PDT, the photons are distributed in a spherical shape by utilizing MCML simulation at $t \sim 60$ s

The photodynamic doses were computed at visible light of $\lambda = 580nm$ in the central cross-section of the blood sample model (the dotted bold black font), as shown in Fig. 11. Note that the threshold dose $D_{th} = 8.6 \times 10^{17}$ photon/g is

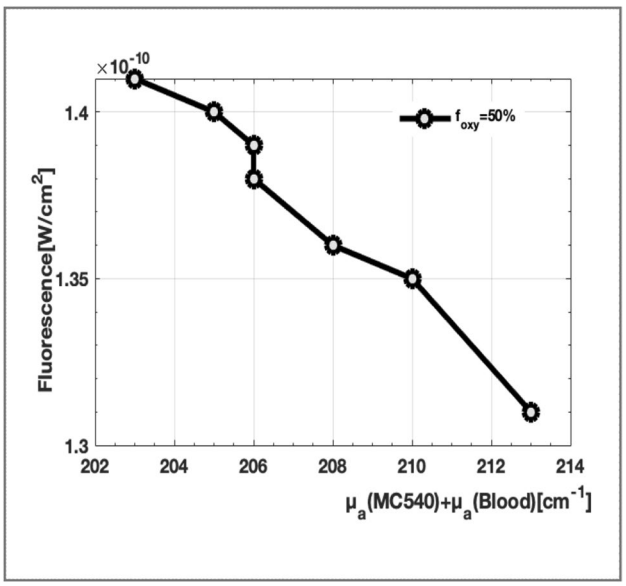

Fig. 10 Simulation of tissue phantoms/blood with the addition of photosensitizer: relationship between the fluence rates and absorption coefficient (μa) including the MC540 with different concentrations of oxygen in the blood ($f_{oxy} = 50\%$, 53%, 55%, 60%, 65%, and 70%)

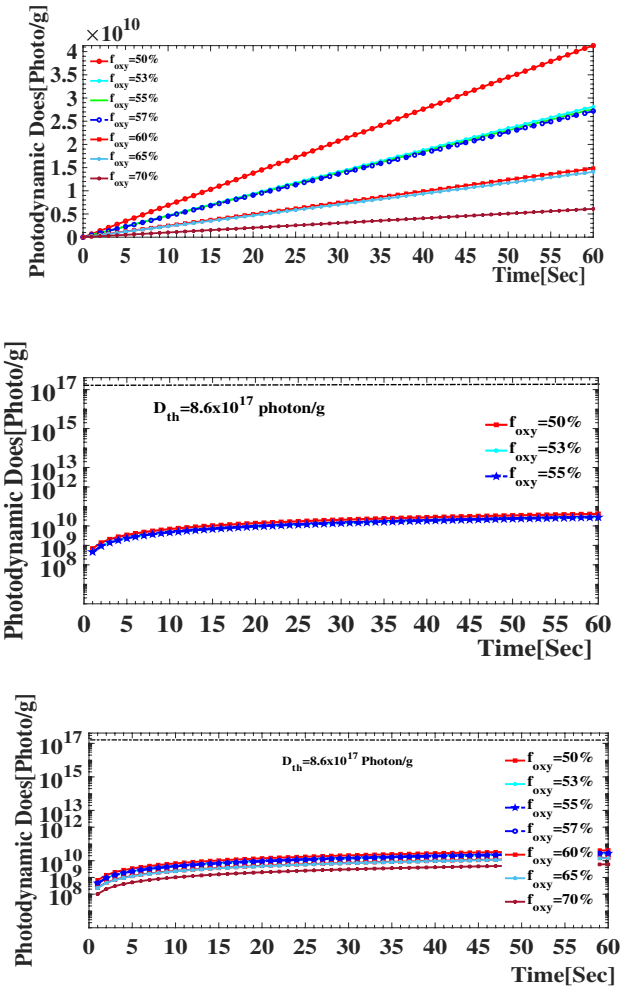

Fig. 11 Relationship between the time (s) and the photodynamic dose (photon/J) at different ratios of concentration of oxygen $f_{oxy} = 50\%$, 53%, 55%, 57%, 60%, 65%, and 70% and photosensitizer MC540 at $C_{MC540} = 30$ μM during $t \sim 60$ s: the maximum photodynamic dose (photon/g) was attained at the maximum exposure time of ~ 60 s, which corresponds to the largest dose ~ at $f_{oxy} = 50\%$, whereas the lowest dose was obtained at $f_{oxy} = 70\%$ and the concentration oxygen dose depends on the treatment

taken from the previous report [41]. The concentration of oxygen at the dose $f_{oxy} = 50\%$ versus the concentration dose $4.6 \times 10^{10} photon/g$ shows the dose factor in the simulated treatment in this study (see Fig. 11). As expected, the saturation value of oxygen of $f_{oxy} = 70\%$ had the greatest value compared with other values of oxygen in the blood. The results show the treatment of a blood sample exposed to the visible light of 580 nm according to a prior study [12], and the target was not achieved at the threshold dose, as indicated in Fig. 11. The maximum value appeared at $f_{oxy} = 50\%$ and $D = 4.6 \times 10^{10} photon/g << D_{th}$.

Increments of the source power from $P = 10mW$ to $P = 30mW$ were used to increase $PD_T = 8.641 \times 10^{17}$ photon/g to $PD_T = 8.67 \times 10^{17}$ photon/g at time

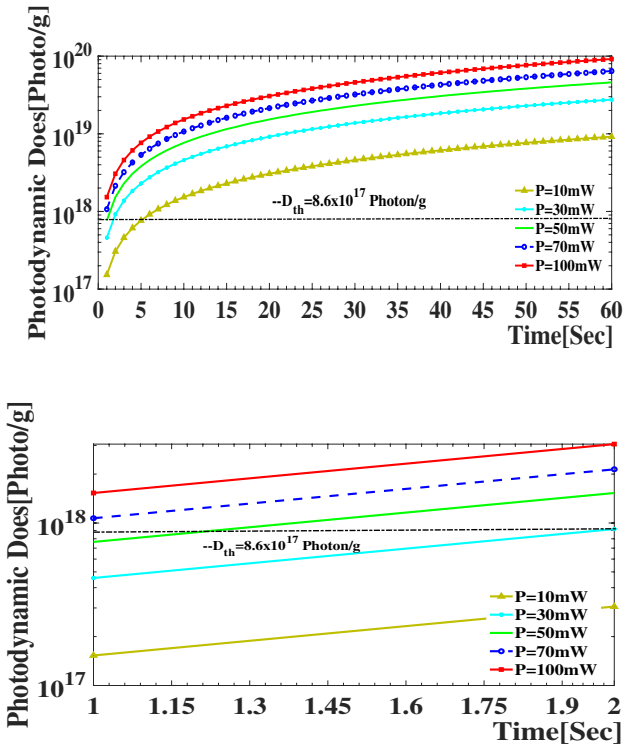

Fig. 12 Photodynamic dose in a human blood sample with $f_{oxy}=50\%$: the dashed line represents the generated threshold dose $D_{th}\sim 8.6\times 1017$ photon/g, and the other lines show a range between the highest and lowest PDD at the surface with $Z=0$ cm obtained at different values of the source powers ($P=10$, 30, 50, 70, and 100 (mW)) with $C_{MC540}=30$ μM

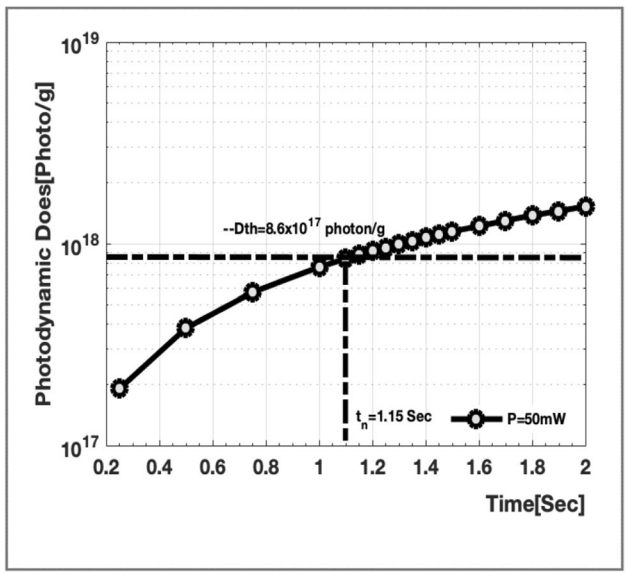

Fig. 13 Dose production in units of photons/g absorbed by the photosensitizer MC540 in the blood ($f_{oxy}=50$) as a function of time at $P=50$ mW: the threshold photodynamic dose is assumed to be $D_{th}\sim 8.6\times 1017$ photon/g, which is absorbed by the photosensitizer, and it is indicated by a horizontal line and the maximum depth achieved at the time of the treated zone of necrosis (depth of $z_n=63$ μm)

$t_n \sim 5.65-1.89s$. However, the maximum power increases in the blood for laser powers between $P=50$ and 70 mW ranged from $PD_T = 8.79\times 10^{17} - 8.88\times 10^{17}$ photon/g at $t_n \sim 1.15-0.7s$, respectively. When different powers of $P=(10,30,50,70,and100[mW])$ are used under the same conditions, the PDT is delivered along the lower power: $P<10$ mW. There is no immediate effect on the treatment, and it may take longer, as shown in Fig. 12. However, at higher values of approximately $P>30$ mW, the treatment continues gradually, and, at $P=50$ mW, an appropriate LD is delivered to achieve the treatment. This protocol enabled the treatment to be completed in a reasonably short time frame approaching ~ 1.15 s.

For the simulations of PDD, a toxic threshold is included and approximates the number of photons that must be absorbed for an effective PDT outcome. The value of $D_{th}\sim 8.6\times 10^{17}$ photons cm^3 is based on Photofrin in liver tissue, where Photofrin is an alternative photosensitizer. For a toxic threshold, the typical values are in the region of $D_{th}\sim 10^{17}-10^{19}$ photons cm^3; therefore, the applied toxic threshold is an approximation of the required dose [46].

Blood treatment zone z_n

Figure 13 shows the various PDD change profiles as a function of the time in the blood sample models under the same conditions as those used before. The maximum power increases by using the visible light for laser powers at $P=10,30,50,70,and100mW$, respectively. The simulation was designed to determine the power source at which the LD was the most efficient for the PDT treatment. The results obtained from the model suggest $P=50$ mW, and the light was delivered to a good depth in the blood treatment at a specified simulation treatment time of ~60 s.

Normal blood response to PDT

Surface treatment was applied to a blood sample at the time of treatment $t=1$ min with a total treatment LD of $3.83\sim Jcm^{-2}$ for $P=50$ mW. Therefore, the treatment was applied with necrosis at approximately $t_n\sim 1.15s$, and the laser light had a wavelength of $\lambda=580nm$, which is an effective treatment for blood cancer at the depth of necrosis $z_n=63\mu m$ (see Fig. 13). The effect of PDT on normal blood can be seen by providing MC540 at light of $\lambda=580nm$. First, the blood sample was treated with $C_{MC540}=30$ μM, as depicted in Fig. 2.

Figure 14 shows the selective necrosis of blood and the effect of phototherapy treatment on the blood by using

MC540 irradiation at 60 s as well as a visible light of $\lambda = 580nm$. At an irradiation time of $t = 60s$, all six doses of light (LD = 0.76, 1.52, 2.29, 3.05, 3.83, 4.58, and 5.35 Jcm^{-2}) resulted in the presence of regions of extensive necrosis at different necrosis times (see Table 5). The marked necrosis could be induced at LD = 1.52 J cm^{-2}. However, the increased LD = 3.05 J cm^{-2} conducted to a much wider range of LD. After delivering light at doses greater than LD = 2.4 J cm^{-2}, normal tissue toxicity was evident. For the blood sample that received the highest dose of $LD_{max} = 5.35$ J cm^{-2} at the highest fluence rate of $F = 89.17mWcm^{-2}$, it was possible to obtain blood necrosis at a depth of $z_n = 158$ μm during the time of necrosis of $t_n = 0.85$ s ($f_{oxy} = 50\%$, $D = 8.794 \times 10^{17} photon/g$). The blood sample was irradiated at three doses of high total energy of $LD = 1.52, 2.29, and 3.05 Jcm^{-2}$ at fluence rates of $F = (25.47, 38.21, and 50.95 mWcm^{-2})$. This can demonstrate a reduced degree of injury ($z_n = 13, 23, and 28 \mu m$) at necrosis time ($t_n = 5.65$, 1.89, and 1.42 s). At the threshold dose, the PDD surface dose values as a function of LD are determined at seven source powers. Figure 14a demonstrates that the PDD deposition is indicated at $LD = 3.83 Jcm^{-2}$ in the blood located at a depth of $z_n = 63$ μm and $P = 50$ mW. In addition, Fig. 14d shows the time effect of necrosis and its relation to the dose of light, which decreases slowly at higher values of LD and finally converges at the endpoint during t_n = 0.76 s. This is caused by the change in the speed response rate of the treatment of LD values within $P = 50$ mW.

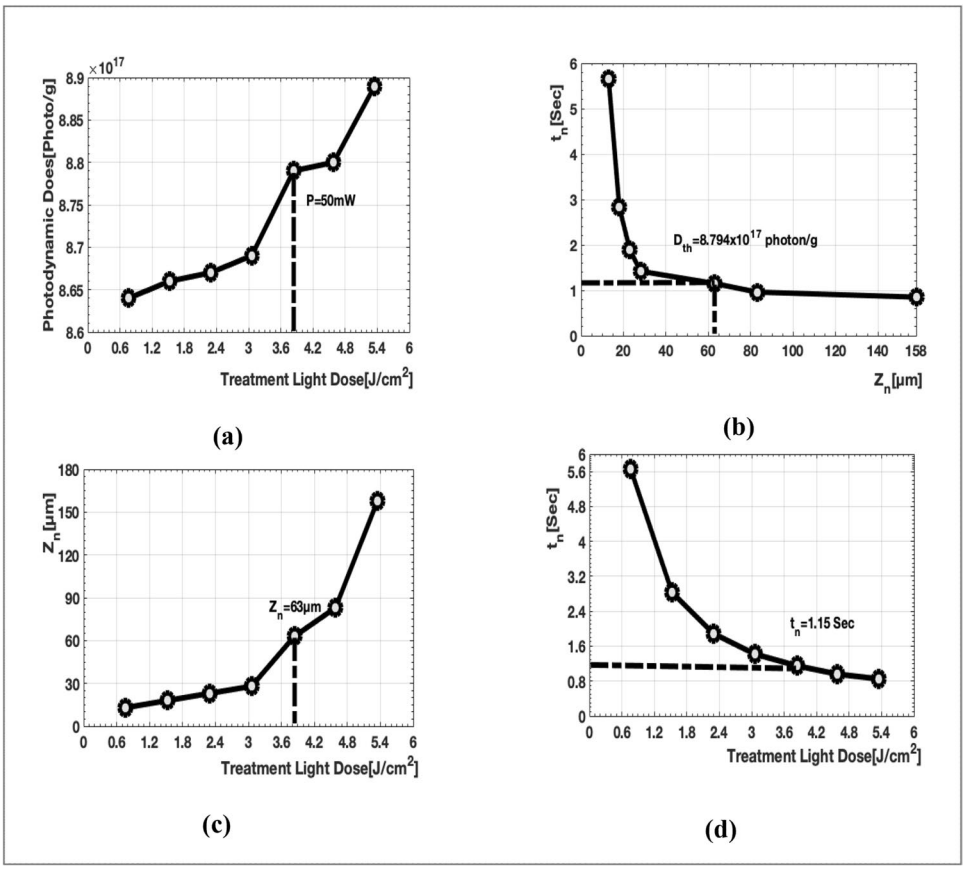

Fig. 14 **a** Simulated PDD for the treatment at different power sources with LD: normal blood necrosis follows various doses of LD (0.76–5.35 Jcm^{-2}) through a period of 60 s to the irradiation light of 580 nm, the normal necrosis decreases at low doses and then begins with actual treatment at LD = 3.83 Jcm^{-2}, and **b**–**d** represent the effect of treatment time at the necrosis regions and the corresponding delivery LD

Table 5 Comparison of the variables that achieve the PDT at the threshold limit of $D_{th} 8.60 \times 10^{17} photon/$ g on the surface at $t \sim 60$ s

Power (P) (mW)	$10mW$	$20mW$	$30mW$	$40mW$	$50mW$	$60mW$	$70mW$
Light dose (LD) [Jcm^{-2}]	0.764	1.528	2.29	3.05	3.83	4.58	5.35
Threshold photodynamic dose (PD_T)	8.641×10^{17}	8.65×10^{17}	8.67×10^{17}	8.68×10^{17}	8.79×10^{17}	8.80×10^{17}	8.88×10^{17}
Time of necrosis (t_n) [s]	5.65	2.83	1.89	1.42	1.15	0.96	0.85
Depth of necrosis (Z_n)[μm]	13	18	23	28	63	83	158

Discussion

Previous studies indicated the importance of the associated concentration ratio of oxygen saturation in hemoglobin and its effect during dosimetry in PDT. Therefore, the accurate oxygen measurements recorded in blood are crucial for the investigation of lesions or leukemia. For this reason, a uniform distribution of light was assumed throughout the blood sample using the photosensitizer MC540. However, the published data on photosensitizer distributions are limited for MC540 used in the blood tumors. Therefore, several researchers performed a basic inspection of the essence of MC540-mediated photodynamic damage for leukemia cells by examining the effects of MC540-sensitizer [47]. A recent study showed that the contribution of MC540 was useful for the treatment of leukemia. Hence, several applications of MC540-mediated photodynamic therapy (MC540-PDT) were examined for the purging of autologous hematopoietic stem cell grafts. They have been employed into human peripheral blood lymphocytes [48].

PDT's effect on blood oxygenation was studied as a function of changes in blood hemoglobin oxygen saturation (f_{oxy}) through the predicted blood response to the light. The excitation was performed using a 580-nm output from the point source at a diameter spot $r = 5mm$ by considering a surface irradiation of a normal blood sample. The geometrical diagram for the spatial distribution of light 2D $[50 \times 50]cm^2$ is depicted in Fig. 8. The blood sample model was simulated at different concentrations of oxygen ($f_{oxy} = 50\%$, 53%, 55%, 57%, 60%, 65%, and 70%). Different concentrations demonstrated that the higher the saturation, the greater the depth of the penetration of light. This resulted in more-prominent spectra at a concentration of $f_{oxy} = 70\%$, as shown in Fig. 4.

MC simulations predicted that an LD of 2.29 J cm^{-2} delivers the threshold dose at a depth of $z_n = 23\mu m$, while a slightly lower LD of 1.52 J cm^{-2} induces a predicted necrosis depth at only $z_n = 18\mu m$. However, an increase of the LD to 3.83 J cm^{-2} yields a much deeper blood necrosis at a depth of $z_n = 63\mu m$. Such a large difference in tissue effect as a function of small changes in LD may explain the variation responses of patients treated with PDT [48]. For any simulated LDs up to $<$ LD = 2.29 J cm^{-2}, the threshold of damage to the blood layer is probably much lower than the threshold for necrosis. The dosimetry equations predicted that approximately LD = 3.83 J cm^{-2} at $P = 50mW$ is sufficient to achieve the desired therapeutic effect for a target thickness of 35 μM. This could potentially injure necrosis or destroy the blood.

Finally, in human blood therapy, the response of blood with concentrations of the photosensitizer MC540 to the fluence rate of $F = 63.69mWcm^{-2}$ was tested with LD to an irradiation time of $t = 60$ s. As it is apparent in Fig. 14, the PDT may be required to deliver LD = 3.83 J/cm^2 into necrosis blood at 63 μm during $t_n = 1.15$ s for the treatment. This can be achieved by using a point source for the laser light with a spherical diffuser and can greatly reduce time during the operation needed for the PDT. To control malignant cells via the combination of radiotherapy and modern biological techniques, PDT continues to adhere to the improved control of blood tumors through selective local of a blood tumor adjacent to the uninfected region. This may aid to overcome the persistent issue of blood tumors without provoking unacceptable harm to the surrounding blood that works regularly. It is then possible to have a safe and effective treatment with a good surface therapeutic plan by using lasers. Thus, the technique can be used for the optimization of treatment parameters and protocols.

Conclusion

In summary, the superficial treatment plan simulated the light propagation via a blood sample model. A point source possessing a spherical distribution was focused on the surface of normal blood sample, while LDs were set up to 3.83 J cm^{-2}. The relationship between the absorption spectrum of MC540 and fluorescence rate was determined to estimate the concentration in the blood, which is provided at the maximum absorption of light to achieve the treatment. Accordingly, the oxygen saturation of hemoglobin in the blood was estimated to be $f_{oxy} = 50\%, 53\%, 55\%, 57\%, 60\%, 65\%, and 70\%$ at wavelength of 580 nm. During the PDT treatment, the oxygen saturation rate of $f_{oxy} = 50\%$ was found to be more responsive than $f_{oxy} = 70\%$ in the blood. This can lead to increasing the probability of survival, i.e., at a 20% response rate, a higher probability exists for a better treatment and faster necrosis death of the cell. This leads to the correlation between the reduction in PDT and arising relative-oxygen concentration $f_{oxy}\%$. These results propose that monitoring the PDT can induce variations in tumor oxygenation and may be an advantageous prognostic indicator. For all cases, the change in the concentration of oxygen minimally affected the scattering characteristics. The MC simulations exhibited that the existence of these concentrations of oxygen ameliorated the simulation of fluence levels in blood. In addition, the results suggested that the source power increases and should not exceed 50 mW to achieve the dose needed for the surface treatment at the threshold dose and to provide an effective treatment for depth PDT with blood necrosis. A relationship was found between the surface treatment of the blood sample and its effect on the local damage around the necrosis depth at different source powers up to 70 mW. At a threshold dose of $D_{th} 8.6 \times 10^{17}$ photon/g, corresponding to the time $t_n = 1.15$ s, this may help for the evaluation of an efficient treatment by including the photochemical reaction with MC540. Hence, the results suggest that the

concentration of $C_{MC540} = 30\mu M$ may further improve the treatment guidance. To reach the role in the blood (leukemia) treatment, the determination of a light delivery protocol procured a maximal therapeutic impact for achieving blood necrosis at $Z_n = 63$ µm. Finally, the MCML simulations clearly demonstrated the importance of selecting the right light source to provide the ideal deliverance of light to establish blood necrosis. These results offer decisive data towards the determination of proper light dosimetry parameters for an intended light-based biomedical application of concentrations of oxygen.

Declarations

Ethical approval All authors contributed equally for the computation and writing of manuscript.

Informed consent No informed consent process was necessary.

Conflict of interest The authors declare no competing interests.

References

1. Santos D, Ferreira A et al (2019) Photodynamic therapy in cancer treatment-an update review. J Cancer Metastasis Treat 5(25):10–20517
2. Jarvi Mark T et al (2011) The influence of oxygen depletion and photosensitizer triplet-state dynamics during photodynamic therapy on accurate singlet oxygen luminescence monitoring and analysis of treatment dose response. Photochem Photobiol 87(1):223–234
3. Baochang L, Farrell TJ, Patterson MS (2012) Comparison of noninvasive photodynamic therapy dosimetry methods using a dynamic model of ALA-PDT of human skin. Phys Med Biol 57(3):825
4. Ferraz RCMC et al (2009) Determination of threshold dose of photodynamic therapy to measure superficial necrosis. Photomed Laser Surg 27(1):93–99
5. Rocha LB et al (2015) Elimination of primary tumours and control of metastasis with rationally designed bacteriochlorin photodynamic therapy regimens. Eur J Cancer 51(13):1822–1830
6. Atzpodien J, Gulati SC, Clarkson BD (1986) Comparison of the cytotoxic effects of merocyanine-540 on leukemic cells and normal human bone marrow. Can Res 46(10):4892–4895
7. Qiu K, Sieber F (1992) Merocyanine 540-sensitized photoinactivation of leukemia cells: effects of dose fractionation. Photochem Photobiol 56(4):489–493
8. Farina B et al (1999) MC simulation of light fluence in tissue in a cylindrical diffusing fibre geometry. Phys Med Biol 44(1):1
9. Wang HW et al (2005) Broadband reflectance measurements of light penetration, blood oxygenation, hemoglobin concentration, and drug concentration in human intraperitoneal tissues before and after photodynamic therapy. J Biomed Opt 10(1):014004
10. Herrmann BH, Hornberger C (2018) Monte-Carlo simulation of light tissue interaction in medical hyperspectral imaging applications. Curr Dir Biomed Eng 4(1):275–278
11. Chatterjee S, Phillips JP, Kyriacou PA (2016) Monte Carlo investigation of the effect of blood volume and oxygen saturation on optical path in reflectance pulse oximetry. Biomed Physics Eng Express 2(6):065018
12. Alotaibi S, Smith WA (2017) A biophysical 3D morphable model of face appearance. In Proceedings of the IEEE International Conference on Computer Vision Workshops (pp. 824–832). https://doi.org/10.1109/ICCVW.2017.102
13. Chen S et al (2015) Monte Carlo investigation of optical coherence tomography retinal oximetry. IEEE Trans Biomed Eng 62(9):2308–2315
14. Haj-Hosseini N (2012) Fluorescence spectroscopy for quantitative demarcation of glioblastoma using 5-aminolevulinic acid. Linköping University Electronic Press, Diss
15. Kalyanaraman B et al (1987) Photodynamic action of merocyanine 540 on artificial and natural cell membranes: involvement of singlet molecular oxygen. Proc Natl Acad Sci 84(9):2999–3003
16. Zhang S, Zhang Z, Jiang D (2002) Photodynamic therapy of different photosensitizers in leukemia. In International Workshop on Photonics and Imaging in Biology and Medicine (Vol. 4536, pp. 54–63). International Society for Optics and Photonics. https://doi.org/10.1117/12.462525
17. Nowak-Sliwinska P et al (2006) Verteporfin, photofrin II, and merocyanine 540 as PDT photosensitizers against melanoma cells. Biochem Biophys Res Commun 349(2):549–555
18. Hoebeke M, Piette J, van de Vorst A (1990) Viscosity-dependent isomerization and fluorescence yields of merocyanine 540. J Photochem Photobiol 4:273–282
19. Ormond AB, Freeman HS (2013) Dye sensitizers for photodynamic therapy Materials 6(3):817–840
20. Dixon JM, Du H (2020) Merocyanine 540 - OMLC citation. How and when to reference. Retrieved from https://omlc.org/spectra/PhotochemCAD/html/066.html
21. Zhu TC, Finlay JC (2006) Prostate PDT dosimetry. Photodiagn Photodyn Ther 3(4):234–246
22. van Straten D et al (2017) Oncologic photodynamic therapy: basic principles, current clinical status and future directions. Cancers 9(2):19
23. Zhu TC , Liu B , Kim MM , McMillan D , Liang X, Finlay JC, Busch TM (2014) Comparison of singlet oxygen threshold dose for PDT. In: Optical Methods for Tumor Treatment and Detection: Mechanisms and Techniques in Photodynamic Therapy XXIII. International Society for Optics and Photonics. Proceedings Volume 8931. https://doi.org/10.1117/12.2039719
24. Uzdensky AB et al (2015) Photodynamic therapy: a review of applications in neurooncology and neuropathology. J Biomed Opt 20(6):061108
25. van Leeuwen-van Zaane F (2014) Fiber optic spectroscopy for the optimization of photodynamic therapy. Erasmus University Rotterdam. http://hdl.handle.net/1765/51078
26. Campbell CL (2016) Under the skin: Monte Carlo radiation transfer modelling of photodynamic therapy. Doctoral thesis, University of St Andrews. Google Scholar. https://research-repository.standrews.ac.uk/handle/10023/9899
27. Periyasamy V, Pramanik M (2014) Monte Carlo simulation of light transport in turbid medium with embedded object—spherical, cylindrical, ellipsoidal, or cuboidal objects embedded within multilayered tissues. J Biomed Opt 19(4):045003
28. Jacques SL (1998) Light distributions from point, line and plane sources for photochemical reactions and fluorescence in turbid biological tissues. Photochem Photobiol 67(1):23–32
29. Milanic M, Majaron B (2011) Three-dimensional Monte Carlo model of pulsed-laser treatment of cutaneous vascular lesions. J Biomed Opt 16(12):128002

30. Burns JM et al (2016) Optical properties of biomimetic probes engineered from erythrocytes. Nanotechnology 28(3):035101
31. Prahl SA (1989) A Monte Carlo model of light propagation in tissue. In Dosimetry of laser radiation in medicine and biology. In: Proceedings International Society for Optics and Photonics 10305:1030509. https://doi.org/10.1117/12.2283590
32. Periyasamy V, Pramanik M (2017) Advances in Monte Carlo simulation for light propagation in tissue. IEEE Rev Biomed Eng 10:122–135
33. Niemz MH (2007) Laser-tissue interactions. Springer-Verlag, Berlin Heidelberg, pp 78–79
34. Wilson BC, Patterson MS (2008) The physics, biophysics and technology of photodynamic therapy. Phys Med Biol 53(9):R61
35. Driver I, Lowdell CP, Ash DV (1991) In vivo measurement of the optical interaction coefficients of human tumours at 630 nm. Phys Med Biol 36(6):805
36. Angell-Petersen E, Hirschberg H, Madsen SJ (2007) Determination of fluence rate and temperature distributions in the rat brain; implications for photodynamic therapy. J Biomed Opt 12(1):014003
37. Jacques SL (2010) How tissue optics affect dosimetry of photodynamic therapy. J Biomed Opt 15(5):051608
38. Bargo PR (2004) Optical measurements for quality control in photodynamic therapy. PhD thesis, Oregon Health & Science University
39. Campbell CL et al (2015) Monte Carlo modelling of daylight activated photodynamic therapy. Phys Med Biol 60(10):4059
40. Zhu TC, Finlay JC, Wilson B (2005) TH-A-T-6C-01: Photodynamic Therapy: Fundamentals and Dosimetry. Med Phys 32(6).https://doi.org/10.1118/1.1999750
41. Campbell CL et al (2016) Monte Carlo modelling of photodynamic therapy treatments comparing clustered three dimensional tumour structures with homogeneous tissue structures. Phys Med Biol 61(13):4840
42. Chen Q et al (1996) Damage threshold of normal rat brain in photodynamic therapy. Photochem Photobiol 64(1):163–167
43. Ferraz RCMC et al (2009) Determination of threshold dose of photodynamic therapy to measure superficial necrosis. Photomed Laser Surg 27(1):93–99
44. O'Brien JM et al (1992) Merocyanine 540-sensitized photoinactivation of enveloped viruses in blood products: site and mechanism of phototoxicity. Blood 80(1):277–285
45. Gaffney DK, Sieber F (1990) Merocyanine 540-sensitized photoinactivation of soluble and membrane-bound enzymes in L1210 leukemia cells. Can Res 50(24):7765–7769
46. Gaffney DK, Sieber F (1990) Merocyanine 540-sensitized photoinactivation of soluble and membrane-bound enzymes in L1210 leukemia cells. Cancer research 50(24):7765–7769. https://pubmed.ncbi.nlm.nih.gov/2174731/
47. Daziano JP (2012) Photochemically generated elemental selenium forms conjugates with serum proteins that are preferentially cytotoxic to leukemia and selected solid tumor cells. Photochem Photobiol 88(2):448–460
48. Traul DL, Sieber F (2015) Inhibitory effects of merocyanine 540-mediated photodynamic therapy on cellular immune functions: a role in the prophylaxis of graft-versus-host disease? J Photochem Photobiol, B 153:153–163
49. Fink C, Enk A, Gholam P (2015) Photodynamic therapy–aspects of pain management. JDDG: J der Deutschen Dermatologischen Gesellschaft 13(1):15–22

Terms and Conditions

Springer Nature journal content, brought to you courtesy of Springer Nature Customer Service Center GmbH (“Springer Nature”).
Springer Nature supports a reasonable amount of sharing of research papers by authors, subscribers and authorised users (“Users”), for small-scale personal, non-commercial use provided that all copyright, trade and service marks and other proprietary notices are maintained. By accessing, sharing, receiving or otherwise using the Springer Nature journal content you agree to these terms of use (“Terms”). For these purposes, Springer Nature considers academic use (by researchers and students) to be non-commercial.
These Terms are supplementary and will apply in addition to any applicable website terms and conditions, a relevant site licence or a personal subscription. These Terms will prevail over any conflict or ambiguity with regards to the relevant terms, a site licence or a personal subscription (to the extent of the conflict or ambiguity only). For Creative Commons-licensed articles, the terms of the Creative Commons license used will apply.
We collect and use personal data to provide access to the Springer Nature journal content. We may also use these personal data internally within ResearchGate and Springer Nature and as agreed share it, in an anonymised way, for purposes of tracking, analysis and reporting. We will not otherwise disclose your personal data outside the ResearchGate or the Springer Nature group of companies unless we have your permission as detailed in the Privacy Policy.
While Users may use the Springer Nature journal content for small scale, personal non-commercial use, it is important to note that Users may not:

1. use such content for the purpose of providing other users with access on a regular or large scale basis or as a means to circumvent access control;
2. use such content where to do so would be considered a criminal or statutory offence in any jurisdiction, or gives rise to civil liability, or is otherwise unlawful;
3. falsely or misleadingly imply or suggest endorsement, approval , sponsorship, or association unless explicitly agreed to by Springer Nature in writing;
4. use bots or other automated methods to access the content or redirect messages
5. override any security feature or exclusionary protocol; or
6. share the content in order to create substitute for Springer Nature products or services or a systematic database of Springer Nature journal content.

In line with the restriction against commercial use, Springer Nature does not permit the creation of a product or service that creates revenue, royalties, rent or income from our content or its inclusion as part of a paid for service or for other commercial gain. Springer Nature journal content cannot be used for inter-library loans and librarians may not upload Springer Nature journal content on a large scale into their, or any other, institutional repository.
These terms of use are reviewed regularly and may be amended at any time. Springer Nature is not obligated to publish any information or content on this website and may remove it or features or functionality at our sole discretion, at any time with or without notice. Springer Nature may revoke this licence to you at any time and remove access to any copies of the Springer Nature journal content which have been saved.
To the fullest extent permitted by law, Springer Nature makes no warranties, representations or guarantees to Users, either express or implied with respect to the Springer nature journal content and all parties disclaim and waive any implied warranties or warranties imposed by law, including merchantability or fitness for any particular purpose.
Please note that these rights do not automatically extend to content, data or other material published by Springer Nature that may be licensed from third parties.
If you would like to use or distribute our Springer Nature journal content to a wider audience or on a regular basis or in any other manner not expressly permitted by these Terms, please contact Springer Nature at

onlineservice@springernature.com